Curvature-driven stability of defects in nematic textures over spherical disks

Xiuqing Duan and Zhenwei Yao[*]

School of Physics and Astronomy, and Institute of Natural Sciences, Shanghai Jiao Tong University, Shanghai 200240, China
(Received 22 March 2017; published 26 June 2017)

Stabilizing defects in liquid-crystal systems is crucial for many physical processes and applications ranging from functionalizing liquid-crystal textures to recently reported command of chaotic behaviors of active matters. In this work, we perform analytical calculations to study the curvature-driven stability mechanism of defects based on the isotropic nematic disk model that is free of any topological constraint. We show that in a growing spherical disk covering a sphere the accumulation of curvature effect can prevent typical $+1$ and $+1/2$ defects from forming boojum textures where the defects are repelled to the boundary of the disk. Our calculations reveal that the movement of the equilibrium position of the $+1$ defect from the boundary to the center of the spherical disk occurs in a very narrow window of the disk area, exhibiting the first-order phase-transition-like behavior. For the pair of $+1/2$ defects by splitting a $+1$ defect, we find the curvature-driven alternating repulsive and attractive interactions between the two defects. With the growth of the spherical disk these two defects tend to approach and finally recombine towards a $+1$ defect texture. The sensitive response of defects to curvature and the curvature-driven stability mechanism demonstrated in this work in nematic disk systems may have implications towards versatile control and engineering of liquid-crystal textures in various applications.

I. INTRODUCTION

Functionalizing the rich variety of self-assembled liquid-crystal (LC) structures represents a trend in LC research [1–4]. Confining LCs in various geometries in the form of droplets [5–7], shells [8–10], and fibers [11,12] using modern microfluidic technology and characterization methods opens the prospect of many application opportunities, and brings new scientific problems related to the creation and engineering of complex director arrangements [4,13–15]. LC textures can be strongly affected by the distribution and type of topological defects, which are singularities in the otherwise continuous LC director field [16–18]. The extraordinary responsiveness of LC makes the manipulation of defects a challenge in applications. Stabilizing defects in two-dimensional LC systems is directly related to arrangement of LC textures [13,16,19,20], fabrication of controllable valency in colloid-LC-based artificial atoms [21–23], modulation of coupled geometries where LC lives [24–30], and relevant applications in active matter systems [31–35]. A prototype model to study the stability mechanism of defects in LC is the isotropic two-dimensional LC disk model with a single elastic constant [36–38]. In a flat freestanding LC disk, defects tend to move swiftly to the boundary to form a boojum texture, which is a two-dimensional version of its namesake in superfluid helium-3 [36,39,40]. A virtual boojum texture with a topological defect outside the sample has been predicted in planar circular LC domains by Langer and Sethna [36], and it has been found to be a local energy extremal [37,38]. Sufficiently strong pinning boundary conditions can stabilize a defect within a circular LC domain [36–38].

Exploring other stability mechanisms of defects in LC samples in addition to imposing boundary conditions constitutes an underlying scientific problem towards versatile control and engineering of LC director arrangement. Confining LC over spherical surfaces can generate various regularly arranged stable defect patterns [8,23,25,41–45]. Vitelli and Nelson have studied two-dimensional nematic order coating frozen surfaces of spatially varying Gaussian curvature, and found the instability of a smooth ground-state texture to the generation of a single defect using free boundary conditions [46]. These results of LC order on closed spheres and topographies with varying curvature show that curvature suffices to provide a stability mechanism for defects even without imposing any pinning boundary condition. However, for LC order on a closed sphere, it is unknown to what extent the appearance of defects is energetically driven, while they must appear as a consequence of the spherical topology. To remove the topological constraint, we study nematic order, the simplest LC order, on a spherical disk. Here we emphasize that, due to the fundamentally distinct topologies of sphere and disk, the appearance of defects on spherical disks is not topologically required; the emergence of defects therein is purely geometrically driven. According to the continuum elasticity theory of topological defects in either LC or crystalline order, the stress caused by defects can be partially screened by Gaussian curvature [17,18,44,47]. Therefore, one expects the appearance of defects on a sufficiently curved spherical disk. It is of interest to identify the transition point for a defect to depart from the boundary of the disk, and illustrate the nature of the transition by clarifying questions such as: Will the defect move rapidly or gradually with the accumulation of curvature effect? Will the defect split as the nematic texture becomes more and more frustrated by the curvature? Once split, will the resulting defects become stable on the spherical disk?

We perform analytical calculations based on the isotropic nematic disk model to address these fundamental problems. This theoretical model may be realized experimentally in Langmuir monolayers [38,48–50] and liquid-crystal films [36,51] deposited at the surface of water droplets whose curvature is controllable by tuning the droplet size [4]. Flat space experiments in these two-dimensional monolayer systems at air-water interface have revealed stable liquid-crystal phases [48,50,51].

In this work, we first discuss the two instability modes of a $+1$ defect over a flat disk, either sliding to the boundary or splitting to a pair of $+1/2$ defects. By depositing the nematic order over a spherical surface, we analytically show that bending deformation of a director field is inevitable everywhere, which implies the appearance of defects to release the curvature-driven stress. By comparing a flat and a spherical nematic disk of the same area, both containing a $+1$ defect at the center, we derive for the analytical expression for the difference of the Frank free energy, and show that the spherical disk always has higher energy. However, when the $+1$ defect deviates from the center of the disk, the free energy curves become qualitatively different for flat and spherical disks when the disk area exceeds some critical value. Specifically, the equilibrium position of the $+1$ defect rapidly moves from the boundary to the center of the spherical disk in a narrow window of the disk area, exhibiting the first-order phase-transition-like behavior. For the pair of $+1/2$ defects by splitting a $+1$ defect, we further show the curvature-driven alternating repulsive and attractive interactions between the two defects. When the spherical cap occupies more area over the sphere, the pair of $+1/2$ defects tend to approach until merging to a $+1$ defect texture. The recombination of the pair of $+1/2$ defects into a $+1$ defect is consistent with the result of the $+1$ defect case. These results demonstrate the fundamentally distinct scenario of defects in a spherical disk from that on a planar disk. We also briefly discuss the cases of nematic order on hyperbolic disks. In this work, the demonstrated distinct energy landscape of LC defects created by curvature is responsible for the stability of defects, and may have implications in the design of LC textures with the dimension of curvature.

II. MODEL AND METHOD

In the continuum limit, the orientations of liquid-crystal molecules lying over a disk are characterized by a director field $\mathbf{n}(\mathbf{x})$ that is defined at the associated tangent plane at $\mathbf{x}$. The equilibrium nematic texture is governed by minimizing the Frank free energy [17]

$$F = \int_D f \, dA + \lambda(\mathbf{n}^2 - 1), \tag{1}$$

where the integration is over the disk D. The Frank free energy density

$$f = \tfrac{1}{2}K_1(\mathrm{div}\,\mathbf{n})^2 + \tfrac{1}{2}K_3(\mathbf{n} \times \mathrm{curl}\,\mathbf{n})^2, \tag{2}$$

where K_1 and K_3 are the splay and bending rigidities, respectively. The Lagrange multiplier λ is introduced to implement the constraint of $\mathbf{n} \cdot \mathbf{n} = 1$. In general, λ is a function of coordinates. The twist term $(\mathbf{n} \cdot \mathrm{curl}\,\mathbf{n})^2$ vanishes in nematics confined on a sphere (see Appendix B). Equation (2) has been widely used to analyze the deformation in nematic phases. For nematics on curved surfaces, the operators of divergence and curl in the Frank free energy are promoted to be defined on the curved manifold and carry the information of curvature. Note that the curl operator relies on the extrinsic geometry of the surface [52]. Note that the Frank free energy model in Eq. (2) describes the distortion free energy of uniaxial nematics. A formalism based on the tensorial nematic order

parameter has been proposed to characterize the distortion of both uniaxial and biaxial nematics and defects therein [53,54].

We work in the approximation of isotropic elasticity with $K_1 = K_3$. Under such an approximation, one can show that the free energy is invariant under the local rotation of the director field by any angle, whether the disk is planar or curved (see Appendix A). In other words, the energy degeneracy of the system becomes infinite when $K_1 = K_3$. Such configurational symmetry is broken when the ratio K_1/K_3 is deviated from unity. While the states selected by the differential in the values for K_1 and K_3 are of interest in other contexts such as in the ground states of spherical nematics [44], here we work in the isotropic regime to highlight the curvature effect of substrates on the configuration of nematics.

The general Euler-Lagrange equation of the Frank free energy on a curved surface $\mathbf{x}(u^1, u^2)$ is

$$\partial_j \frac{\partial f}{\partial\left(\frac{\partial n_i}{\partial u^j}\right)} + \frac{\partial_j \sqrt{g}}{\sqrt{g}} \frac{\partial f}{\partial\left(\frac{\partial n_i}{\partial u^j}\right)} - \frac{\partial f}{\partial n_i} = -\lambda n_i, \tag{3}$$

where $i, j = 1, 2$, and g is the determinant of the metric tensor. The second term in Eq. (3) is due to the spatially varying g. The nematic textures studied in this work are solutions to Eq. (3).

To characterize defects that are named disclinations in a two-dimensional director field, we perform integration of the orientation θ of the director $\mathbf{n}$ with respect to any local reference frame along any closed loop Γ:

$$\oint_\Gamma d\theta = k\pi, \tag{4}$$

where k is nonzero if Γ contains a defect. Unlike in a vector field where k can only be integers, two-dimensional nematics supports both integer and half-integer disclinations due to the apolarity of liquid-crystal molecules, i.e., $\mathbf{n} \equiv -\mathbf{n}$.

III. RESULTS AND DISCUSSION

We first discuss the case of nematics on a planar disk. It is straightforward to identify the following solution to the Euler-Lagrange equation:

$$\mathbf{n} = \cos(\varphi + \theta_0)\mathbf{e}_1 + \sin(\varphi + \theta_0)\mathbf{e}_2, \tag{5}$$

where $\varphi = \arctan(y/x)$ is the polar angle, θ_0 is a constant, and $\mathbf{e}_i$ is the unit basis vector in Cartesian coordinates. The strength of the defect located at the origin of the coordinates is $+1$. The associated Lagrange multiplier is $\lambda = K_1/(x^2 + y^2)$. The contributions to the splay and bending terms in the free energy density are $K_1\cos^2\theta_0/[2(x^2 + y^2)]$ and $K_3\sin^2\theta_0/[2(x^2 + y^2)]$, respectively. When θ_0 increases from 0 to $\pi/2$, the $+1$ defect transforms from the radial (pure splay) to the azimuthal (pure bending) configurations. In this process, the sum of the splay and bending energies is an invariant under the isotropic elasticity approximation. The total free energy of the configuration in Eq. (5) is

$$F_{+1,p} = \frac{K_1}{2} \iint_{x^2+y^2 \leqslant r_p^2} \frac{1}{x^2 + y^2} dx\,dy, \tag{6}$$

where r_p is the radius of the planar disk.

We show that the $+1$ defect at the center of the planar disk in Eq. (5) is unstable and tends to slide to the boundary of
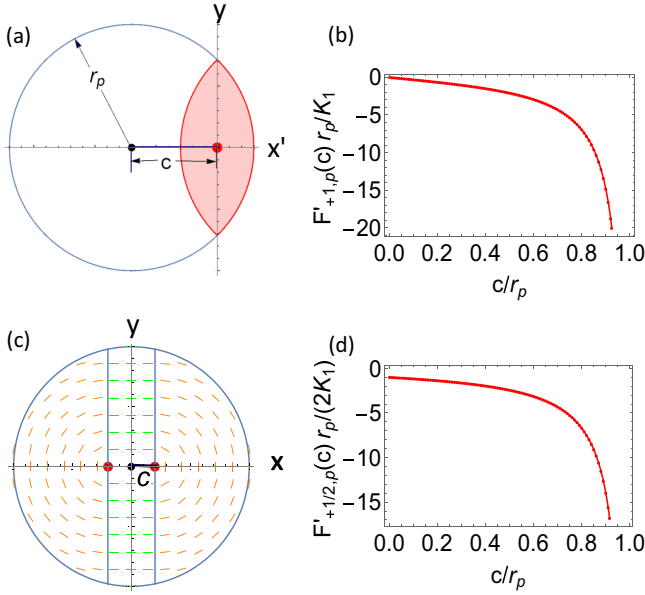
FIG. 1. The configurations and energetics of (a), (b) a single $+1$ defect and (c), (d) a pair of $+1/2$ defects on a planar disk. The defects are represented by red dots. The pair of $+1/2$ defects in (c) are constructed out of a $+1$ defect by inserting a uniform direct field between (indicated by green lines). The negative derivative of the Frank free energy $F(c)$ with respect to c (the position of the defects) indicates that defects tend to slide to the boundary of a planar disk.

the disk. For simplicity, we employ a free boundary condition. Consider a $+1$ defect like in Eq. (5) at $(c,0)$, where $c \leqslant r_p$. Its free energy is

$$F_{+1,p}(c) = \frac{K_1}{2} \iint_{x^2+y^2 \leqslant r_p^2} \frac{1}{(x-c)^2 + y^2} dx dy. \qquad (7)$$

To avoid the singularity point at $(c,0)$ in the evaluation for $F_{+1,p}(c)$, we take the derivative of $F_{+1,p}(c)$ with respect to c. Physically, this procedure returns the force on the defect. While the free energy may diverge, a physical force must be finite. After some calculation, we have

$$F'_{+1,p}(c) = K_1 \iint_{x^2+y^2 \leqslant r_p^2} \frac{x-c}{[(x-c)^2+y^2]^2} dx dy$$

$$= K_1 \iint_{(x'+c)^2+y^2 \leqslant r_p^2} \frac{x'}{(x'^2+y^2)^2} dx' dy, \qquad (8)$$

where variable substitution is applied in the last equality. The integral domain is shown in Fig. 1(a). The defect is located at $x' = 0$ (i.e., $x = c$) and $y = 0$. We see that the integration in the red region returns zero, since the integrand $x'/(x'^2+y^2)^2$ is an odd function of x'. In the rest region where $x' < 0$, the integrand is negative. Therefore, $F'_{+1,p}(c)$ is negative when the defect is deviated from the center of the disk. $F'_{+1,p}(c=0) = 0$. In other words, once deviated from the center of the disk, the defect will slide to the boundary to reduce the free energy of the system. Figure 1(b) shows the numerical result on the dependence of $F'_{+1,p}(c)$ on c/r_p.

An alternative instability mode of the central $+1$ defect in the planar disk is to split into two $+1/2$ defects. Such a process may occur when the interaction energy of the two
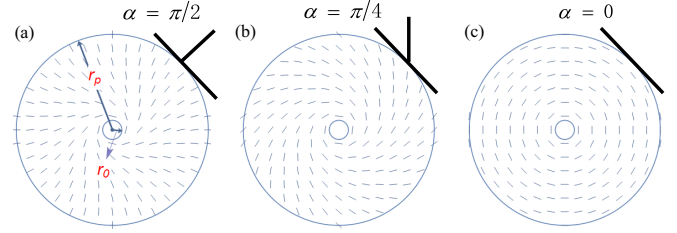
repulsive $+1/2$ defects dominates over the core energy of the defects. To analyze the energetics of the $+1/2$ defects, we construct the director field containing two $+1/2$ defects by cutting and moving apart an azimuthal configuration as shown in Fig. 1(c), where the $+1/2$ defects are represented by red dots. The region between the two half azimuthal configurations is filled with a uniform director field. The Frank free energy of such a configuration is

$$F_{+1/2,p}(c) = 2K_1 \int_0^{r_p-c} dx \int_0^{\sqrt{r_p^2-(x+c)^2}} dy \frac{1}{x^2+y^2}, \quad (9)$$

where the separation between the two defects is $2c$. $F'(0) = -2K_1/r_p < 0$. In Fig. 1(d), we plot $F'_{+1/2,p}(c)$ versus c. The negative sign indicates the repulsive nature of the two $+1/2$ defects. The resulting $+1/2$ defects are ultimately pushed to the boundary of the disk under the repulsive interaction.

In the preceding discussions, we employ the free boundary condition where directors at the boundary do not have preferred orientations. Another important class of boundary condition is to fix the orientation of the molecules at the boundary. Homeotropic and planar liquid-crystal samples are two typical cases, where the directors are perpendicular and parallel to the boundary, respectively. Imposing these pinning boundary conditions over the aster configuration can lead to spiral deformations [13]. Note that a recent study has demonstrated a dynamic consequence of the radial-to-spiral transition of a $+1$ defect pattern in the system of swimming bacteria in a liquid-crystal environment [35]. It is observed that the swimming mode of bacteria changes from bipolar to unipolar when the $+1$ defect pattern becomes spiral. For the general pinning boundary condition that the angle between **n** and the tangent vector at the boundary is α ($\alpha \in [0,\pi/2]$), we obtain the solution to Eq. (3):

$$(n_r, n_\varphi) = [\sin\theta(\alpha), \cos\theta(\alpha)], \qquad (10)$$

where n_r and n_φ are the components of **n** in polar coordinates (r,φ), $\theta(\alpha) = \alpha \ln(r/r_0)/\ln(r_p/r_0)$, r_p and r_0 are the outer and inner radius of the planar disk as shown in Fig. 2. The magic spiral solution in Ref. [13] is a special case of $\alpha = \pi/2$. The associated Lagrange multiplier is $\lambda = (K_1/r^2)\{1 + \alpha^2/[\ln(r_p/r_0)]^2\}$. The configuration of the solution in Eq. (10) is plotted in Fig. 2. The originally straight radial lines deform to spiral curves to satisfy the boundary condition. The Frank free energy of the spiral configuration is

$$F_{\text{spiral}}(\alpha) = \left[1 + \left(\frac{\alpha}{\ln\frac{r_p}{r_0}}\right)^2\right] F_{+1,p}, \qquad (11)$$

FIG. 2. Spiral $+1$ defect patterns subject to typical pinning boundary conditions in a planar nematic disk.

where $F_{+1,p}$ is the free energy of an aster configuration in a planar disk given in Eq. (6). Eq. (11) shows that the boundary effect does not enter the integral of $F_{+1,p}$. The energy cost associated with the spiral deformation conforms to a quadratic law with respect to the angle α and its dependence on the size of disk is relatively weak in a logarithm relation.

Now we discuss two-dimensional nematic texture confined on spherical disks. Consider a director field $\mathbf{n}$ on a sphere $\mathbf{n} = n_1(\theta,\varphi)\mathbf{e}_\theta + n_2(\theta,\varphi)\mathbf{e}_\varphi$, where $\mathbf{e}_\theta$ and $\mathbf{e}_\varphi$ are the unit tangent vectors in spherical coordinates. θ and φ are the polar and azimuthal angles, respectively. We first show that on spherical geometry a director field without any splay and bending deformations is impossible. Topology of the two-dimensional sphere dictates that a harmonic vector field on a sphere is impossible [55]. A vector field is called harmonic if it is divergence free, irrotational, and tangent to the spherical surface. A director field is a vector field with the extra constraints of $|\mathbf{n}| = 1$ and $\mathbf{n} \equiv -\mathbf{n}$. Therefore, it is a topological requirement that one cannot completely eliminate both bending and splay deformations in a director field living on a sphere.

In addition to the above global analysis, we will further show that an irrotational director field is impossible at any point on a sphere. In other words, bending of a director field is inevitable everywhere on a spherical surface. We first present the general expressions for the divergence and curl of a director field over a smooth surface: $\mathrm{div}\,\mathbf{n} = \frac{1}{\sqrt{g}}\partial_i(\sqrt{g}n_i)$ and $\mathrm{curl}\,\mathbf{n} = (\star d\mathbf{n}^\flat)^\sharp$, where $\star$ is the Hodge dual, $\flat$ and $\sharp$ are the musical isomorphisms, d is exterior derivative (see Appendix B). Applying these expressions on a sphere, we have

$$\mathrm{div}\,\mathbf{n} = \frac{\cos\theta}{\sin\theta}\frac{n_1}{R} + \frac{1}{R}\frac{\partial n_1}{\partial\theta} + \frac{1}{R\sin\theta}\frac{\partial n_2}{\partial\varphi}, \quad (12)$$

and

$$\mathrm{curl}\,\mathbf{n} = \frac{1}{R\sin\theta}\left(-\frac{\partial n_1}{\partial\varphi} + n_2\cos\theta + \sin\theta\frac{\partial n_2}{\partial\theta}\right)\mathbf{e_r} \\ - \frac{n_2}{R}\mathbf{e}_\theta + \frac{n_1}{R}\mathbf{e}_\varphi, \quad (13)$$

where $\mathbf{e_r}$ is the unit normal vector. According to Eq. (13), we clearly see that at least one of the last two terms must be nonzero. In contrast, Eq. (12) shows that a divergence-free director field with vanishing splay deformation without any bend deformation is possible. The simplest example is the direction field with only the azimuthal component: $\mathbf{n} = \mathbf{e}_\varphi$. Such a director field is divergence free but with bending deformation. Note that in the calculation for the curl of the director field, we use the condition that the sphere is embedded in three-dimensional Euclidean space. The divergence of the director field does not depend on how the sphere is embedded in the Euclidean space. One can check that the twist term $(\mathbf{n}\cdot\mathrm{curl}\,\mathbf{n})^2 = 0$.

The stability analysis of defects in nematic textures over spherical disks is based on the following expression for the Frank free energy density in spherical
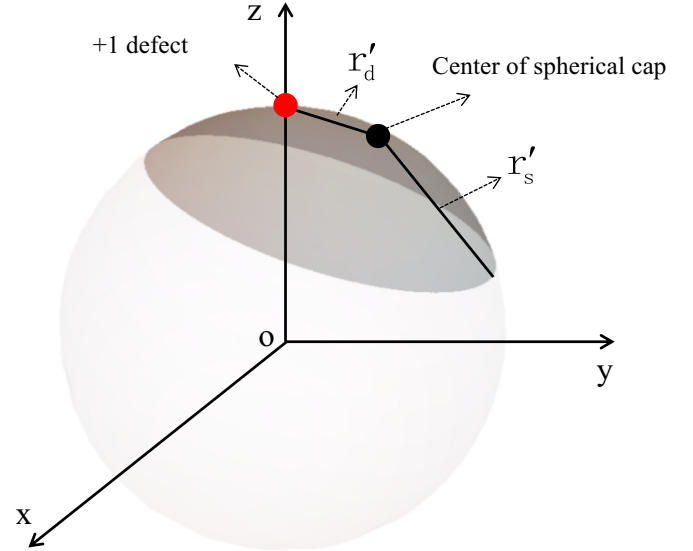

FIG. 3. Schematic plot of a $+1$ defect over a spherical cap. The relative position the defect is characterized by the ratio r'_d/r'_s.

coordinates:

$$f = \frac{K_1}{2R^2}\left(n_1\frac{\cos\theta}{\sin\theta} + \frac{\partial n_1}{\partial\theta} + \frac{1}{\sin\theta}\frac{\partial n_2}{\partial\varphi}\right)^2 + \frac{K_3}{2R^2} \\ \times \left[1 + \frac{1}{\sin^2\theta}\left(n_2\cos\theta + \sin\theta\frac{\partial n_2}{\partial\theta} - \frac{\partial n_1}{\partial\varphi}\right)^2\right]. \quad (14)$$

Note that the first term $K_3/(2R^2)$ in the bending part represents the irremovable bending deformation of a director field over spherical substrates. This term vanishes in the limit of $R \to \infty$. One can check that for a divergence-free director field $\mathbf{n} = \mathbf{e}_\varphi$, $f = K_1/(2R^2\sin^2\theta)$. The singularities at $\theta = 0$ and $\theta = \pi$ correspond to the two $+1$ defects at the north and south poles.

We first discuss if the $+1$ defect can be supported by spherical geometry. All the degenerate nematic configurations containing a $+1$ defect at the center of the spherical cap are characterized by the director field $\mathbf{n} = (c_1,c_2)$, where the constants c_1 and c_2 satisfy $c_1^2 + c_2^2 = 1$. These degenerate states have the same Frank free energy:

$$F_{+1,s} = \frac{K_1}{2}\iint_{\theta,\varphi\in D}\frac{1}{R^2\sin^2\theta}(R^2\sin\theta\, d\theta\, d\varphi) \\ = \frac{K_1}{2}\iint_{\theta,\varphi\in D}\frac{1}{\sin\theta}d\theta\, d\varphi, \quad (15)$$

where the integration is over a spherical cap D with spherical radius R and geodesic radius r_s. And these states are solutions to the Euler-Lagrange equation (see Appendix C).

In order to derive for $F_{+1,s} - F_{+1,p}$, the free energy difference of a $+1$ defect configuration on spherical and planar disks, we introduce the following coordinates transformation. For generality, the Cartesian coordinates of the center of the spherical cap are $(c,0,\sqrt{R^2 - c^2})$ as shown in Fig. 3. The center of the spherical cap is located at the north pole for $c = 0$. The region of the spherical cap is $D = \{(x,y,z)|x^2 + y^2 + z^2 = R^2,(x - c)^2 + y^2 + (z - \sqrt{R^2 - c^2})^2 \leqslant r'^2_s\}$. r'_s is the Euclidean distance from the center to the boundary of the

spherical cap. The area of such a spherical cap is $S = \pi r_s'^2$. Now we construct the stereographic projection from the spherical cap to the plane of equator. Specifically, we draw a line connecting the south pole of the sphere and any point at (x,y,z) or (θ,φ) on the spherical cap. The point on the spherical cap is thus projected to the intersection point (u,v) of this line and the equator plane. The projection is described by the formula

$$(u,v) = \left(\frac{Rx}{z+R}, \frac{Ry}{z+R} \right), \tag{16}$$

or, in terms of spherical coordinates,

$$(u,v) = \left(\frac{R\sin\theta\cos\varphi}{\cos\theta + 1}, \frac{R\sin\theta\sin\varphi}{\cos\theta + 1} \right). \tag{17}$$

The stereographic projection has a convenient geometric property that any spherical cap not containing the point of projection (south pole) is projected to a circular disk on the equator plane:

$$(u - u_0)^2 + v^2 \leqslant r_{eq}^2, \tag{18}$$

where

$$u_0 = \frac{2cR^2}{-r_s'^2 + 2R(R + \sqrt{R^2 - c^2})},$$

and

$$r_{eq}^2 = \frac{r_s'^2 R^2 (4R^2 - r_s'^2)}{\left[r_s'^2 - 2R(R + \sqrt{R^2 - c^2}) \right]^2}.$$

To guarantee that the spherical cap contains the north pole, it is required that $r_s'^2 \geqslant 2R(R - \sqrt{R^2 - c^2})$. Alternatively, $c \leqslant r_s' \sqrt{1 - [r_s'/(2R)]^2}$ for given r_s'. On the other hand, the spherical cap occupies no more than half of a sphere, so $r_s' \leqslant \sqrt{2}R$.

From the Jacobian of the coordinates transformation in Eq. (17)

$$\frac{\partial(u,v)}{\partial(\theta,\varphi)} = \begin{pmatrix} \frac{R\cos\varphi}{1+\cos\theta} & -\frac{R\sin\theta\sin\varphi}{1+\cos\theta} \\ \frac{R\sin\varphi}{1+\cos\theta} & \frac{R\sin\theta\cos\varphi}{1+\cos\theta} \end{pmatrix},$$

and

$$dudv = \left| \frac{\partial(u,v)}{\partial(\theta,\varphi)} \right| d\theta d\varphi = \frac{u^2 + v^2}{\sin\theta} d\theta d\varphi,$$

we finally have

$$\frac{dudv}{u^2 + v^2} = \frac{d\theta d\varphi}{\sin\theta}. \tag{19}$$

We therefore obtain the desired expression for Eq. (15) in the (u,v) coordinates:

$$F_{+1,s} = \frac{K_1}{2} \iint_D \frac{1}{u^2 + v^2} dudv, \tag{20}$$

where the integral domain $D = \{(u,v)|u^2 + v^2 \leqslant r_s'^2 R^2/(4R^2 - r_s'^2)\}$. Note that now the integrands in Eq. (20) and Eq. (6) have the same functional form and can be conveniently compared. A subtle point worth mentioning is that the direct subtraction of Eq. (6) from Eq. (20) will lead to a wrong expression of

$\Delta F = F_{+1,s} - F_{+1,p} = -(\pi/2)K_1 \ln[4 - (r_s'/R)^2]$. One can check that ΔF fails to converge to the expected zero in the limit of $R \to \infty$. Here, the subtlety is from the fact that the integrands in Eq. (20) and Eq. (6) have singularity at the origin point. To eliminate this singularity, one has to cut off the small defect core. The integral domain of Eq. (20) should be $D = \{(u,v)|(a/2)^2 \leqslant u^2 + v^2 \leqslant r_s'^2 R^2/(4R^2 - r_s'^2)\}$, where a is the radius of the defect core. The prefactor of $1/2$ is due to the shrink of the defect size in the previously introduced stereographic projection. The integral domain in Eq. (6) also becomes $a^2 \leqslant x^2 + y^2 \leqslant r_p^2$. To conclude, the change of the total free energy in the deformation of the planar to the spherical nematic disk in the constraint of fixed disk area A_d is

$$\Delta F = F_{+1,s} - F_{+1,p}$$
$$= -\frac{\pi}{2}K_1 \ln \left[1 - \left(\frac{A_d}{4\pi R^2} \right) \right]. \tag{21}$$

We check that ΔF approaches zero in the limit of $R \to \infty$, as expected. Equation (21) shows that $F_{+1,s}$ is always larger than $F_{+1,p}$.

However, it will be shown that a $+1$ defect can be stabilized within a sufficiently curved spherical disk despite the higher energy in comparison with the planar disk case. We analyze the stability of the $+1$ defect from the derivative of the free energy with respect to its position in the disk. The expression for the free energy is rewritten in the new coordinates $\{x,y\}$, where $x = u - u_0$ and $y = v$:

$$F_{+1,s}(c) = \frac{K_1}{2} \iint_{x^2+y^2 \leqslant r_{eq}^2} \frac{1}{(x+u_0)^2 + y^2} dxdy$$
$$= K_1 \int_{-r_{eq}}^{r_{eq}} dx \frac{1}{x+u_0} \arctan \frac{\sqrt{r_{eq}^2 - x^2}}{x + u_0}, \tag{22}$$

where u_0 and r_{eq} are given in Eq. (18). From Eq. (22), we have

$$F_{+1,s}'(c) = K_1 \int_{-r_{eq}}^{r_{eq}} (G_1 + G_2 + G_3) dx, \tag{23}$$

where $G_1 = -[u_0'(c)/(x+u_0)^2]\arctan[\sqrt{r_{eq}^2 - x^2}/(x+u_0)]$, $G_2 = -u_0'(c)\sqrt{r_{eq}^2 - x^2}/[(x+u_0)(u_0^2 - 2u_0x + r_{eq}^2)]$, and $G_3 = r_{eq}r_{eq}'(c)/[(u_0^2 - 2u_0x + r_{eq}^2)\sqrt{r_{eq}^2 - x^2}]$. The G_3 term can be integrated out: $K_1 \int_{-r_{eq}}^{r_{eq}} G_3 dx = K_1\pi r_{eq}r_{eq}'(c)/|u_0^2 - r_{eq}^2|$. Local analysis around the defect at $x = -u_0$ shows that both the G_1 and the G_2 terms are odd functions of x, and can be canceled in the integration of x near the defect. The singularity associated with the defect is therefore removed. Note that $F_{+1,s}'(c)$ is negative in the large R limit, which is consistent with the planar disk case.

Now we analyze zero points of $F_{+1,s}'(c)$. The defect is stable at a zero point where the slope of the $F_{+1,s}'(c)$ curve is positive. With the increase of c, numerical analysis shows that the G_1 term decreases and the G_3 term increases, both starting from zero at $c = 0$. While the G_1 and the G_3 terms are comparable, the G_3 term is much smaller than either of them. The competition of the G_1 and the G_3 terms may lead to another zero point at the $F_{+1,s}'(c)$ curve in addition to the unstable zero point at $c = 0$.
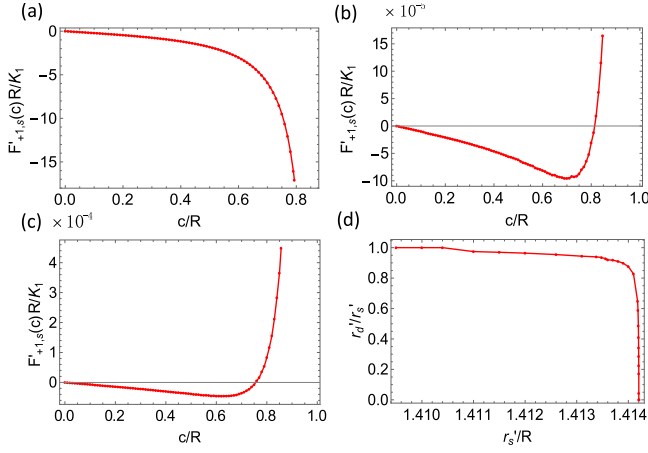
FIG. 4. Stability analysis of a $+1$ defect in a spherical nematic disk. (a)–(c) show the derivative of the Frank free energy $F'_{+1,s}(c)$ versus c at typical values for r'_s/R. The curve starts to develop a stable zero point for the $+1$ defect with the increase of the disk size r'_s. (a) $r'_s/R = 1.0$, (b) 1.414180, and (c) 1.414187. (d) shows the rapid movement of the equilibrium position of the $+1$ defect from the boundary ($r'_d/r'_s = 1$) to the center ($r'_d/r'_s = 0$) of the disk with the increase of the disk size r'_s/R.

In Figs. 4(a)–4(c), we plot $F'_{+1,s}(c)$ versus c at typical values for r'_s. We see that the $F'_{+1,s}(c)$ is negative and monotonously decreasing when the spherical cap is smaller than a critical value. With the increase of r'_s, a second zero point appears at $c = c^*$, where a perturbed defect will be restored to the original equilibrium position. It indicates that the equilibrium position of the defect starts to depart from the boundary of the disk. We introduce the quantity r'_d/r'_s to characterize the equilibrium position of the defect over the spherical cap, where r'_d is the Euclidean distance between the center of the disk and the defect. The variation of the optimal position of the $+1$ defect with the size of the spherical cap is summarized in Fig. 4(d). A pronouncing feature of the r'_d/r'_s vs r'_s/R curve is the rapid decrease from unity to zero when r'_s/R varies by only about 0.1%. It corresponds to the movement of the defect from the boundary to the center of the disk. Such a transition occurs in the narrow window of r'_s when the spherical cap occupies about half of the sphere. Note that the spherical cap becomes a half sphere when $r'_s = \sqrt{2}R$.

Here, it is of interest to compare a $+1$ defect in nematics and a fivefold disclination in a two-dimensional hexagonal crystal on a sphere. Both nematic and crystalline order are frustrated on a sphere, leading to the proliferation of defects. The resulting defects in condensed matter orders are to screen the geometric charge of the substrate surface, which is defined to be the integral of Gaussian curvature. Over a spherical crystal, the topological charge of a fivefold disclination can be screened by a spherical cap of area $A_0/12$ (A_0 is the area of sphere), since 12 fivefold disclinations are required over a spherical crystal by topological constraint [18]. Topological analysis of a spherical nematics shows that a sphere can support two $+1$ defects, so the topological charge of a $+1$ defect can be screened by a spherical cap of area $A_0/2$. Our energetics calculation is consistent with such topological analysis; it is when the spherical cap becomes as large as a half sphere that
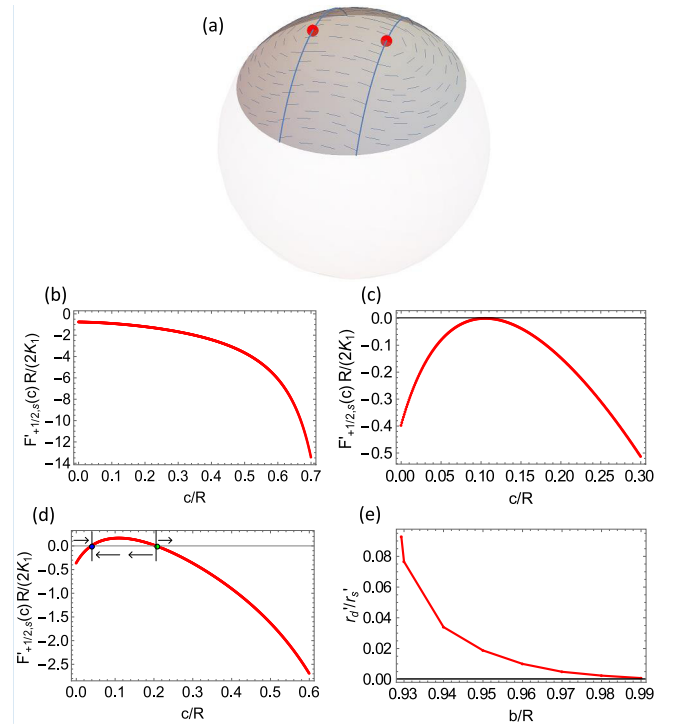

FIG. 5. Stability analysis of a pair of $+1/2$ defects in a spherical nematic disk. (a) is the schematic plot of the defect pair over the spherical disk in gray. (b)–(d) show the derivative of the Frank free energy $F'_{+1/2,s}(c)$ versus c at typical values for b/R. b is the radius of the circular boundary of the spherical cap. A pair of zero points appear in the curve with the increase of the disk size b. (b) $b/R = 0.80000$, (c) 0.92933, and (d) 0.94000. The curvature-driven alternating repulsive and attractive regimes in the $F'_{+1/2,s}(c)$ curve are indicated by the arrows in (d). In (e), we plot the variation of the equilibrium location of the defect pair versus the disk size b/R. r'_d is the Euclidean distance from one of the two defects to the center of the disk. The defect pair merge to form a $+1$ defect ($r'_d/r'_s \to 0$) in the half sphere limit ($b/R \to 1$).

a $+1$ defect will be energetically driven to move to the center of the disk.

We proceed to discuss the split of a $+1$ defect into two $+1/2$ defects over a spherical cap. Like the case of the planar disk, we first construct the director field containing two $+1/2$ defects by cutting an azimuthal $+1$ defect configuration. As shown in Fig. 5(a), the resulting director field on the spherical cap is composed of three parts: the middle uniform region where $\mathbf{n} = (-z/\sqrt{x^2 + z^2}, 0, x/\sqrt{x^2 + z^2})$, and the symmetric azimuthal configurations at the two sides. The origin of the Cartesian coordinates is at the center of the sphere, and the z axis passes through the north pole. The two $+1/2$ defects are indicated by red dots in Fig. 5. Their x coordinates are $x = \pm c$. The center of the spherical cap is at the north pole. The Frank free energy density of the middle uniform configuration is $f = K_1/[2(x^2 + z^2)]$. By putting them together and working in the Cartesian coordinates over the equator plane, we have

$$\frac{F_{+\frac{1}{2},s}}{2K_1} = \iint_{D_1} \frac{1}{x^2 + y^2} dA + \iint_{D_2} \frac{1}{R^2 - y^2} dA, \quad (24)$$

where the surface element of the spherical cap $dA = (R/\sqrt{R^2 - x^2 - y^2})dxdy$, $D_1 = \{(x,y)|y \in [0, \sqrt{b^2 - (x+c)^2}], x \in [0, b-c]\}$, and $D_2 = \{(x,y)|y \in [0, \sqrt{b^2 - x^2}], x \in [0,c]\}$. b is the radius of the circular boundary of the spherical cap. $b = r'_s\sqrt{1 - (r'_s/2R)^2}$.

From Eq. (24), we have

$$\frac{F'_{+\frac{1}{2},s}(c)}{2K_1} = \int_0^{\frac{b-c}{R}} F_1(x)dx + \int_0^{\sqrt{b^2-c^2}} F_2(y)dy, \quad (25)$$

where

$$F_1(x) = R^2(c + Rx)/\{\sqrt{-b^2 + c^2 + R^2 + 2Rcx}$$
$$\times \sqrt{b^2 - (c + xR)^2}[-b^2 + c(c + 2Rx)]\},$$

and $F_2(y) = R/[(R^2 - y^2)\sqrt{R^2 - c^2 - y^2}]$. It is straightforward to show that $F'_{+1/2,s}(0) = -\sqrt{R^2 - b^2}/(Rb) < 0$. It indicates the repulsive interaction between two infinitely close $+1/2$ defects. Numerical evaluation of Eq. (25) shows that when the spherical disk is sufficiently large, the departing $+1/2$ defects can be stabilized within the disk. The plots of $F'_{+1/2,s}(c)$ at typical values for b/R are shown in Figs. 5(b)–5(d). We see that when $b/R > 0.93$, the $F'_{+1/2,s}(c)$ curve starts to hit the horizontal zero line, leading to the two zero points indicated by the blue and the green dots in Fig. 5(d). When the separation between the two defects is smaller than the value at the blue dot or larger than the value at the green dot, they repel with each other. In the regime between the two zero points, the defects attract with each other. The curvature-driven alternating repulsive and attractive regimes in the $F'_{+1/2,s}(c)$ curve are indicated by the arrows in Fig. 5(d). The left zero point (blue dot) represents the equilibrium configuration of the $+1/2$ defects. In Fig. 5(e), we show the variation of the equilibrium position of the $+1/2$ defects with the size of the spherical disk. When the spherical cap occupies more area over the sphere, the distance between the two $+1/2$ defects in the equilibrium configuration shrinks. In the limit of a half sphere, the two $+1/2$ defects merge together, becoming a $+1$ defect. This result is consistent with our previous analysis of the $+1$ defect case, where the optimal position of the $+1$ defect over a half sphere is at the center of the disk.

We proceed to discuss nematic order on Poincaré disk with constant negative Gaussian curvature [56]. The associated metric over a hyperbolic disk with Gaussian curvature K_G is characterized by $ds^2 = 4(dx^2 + dy^2)/(1 + K_Gr^2)^2$, where $r^2 = x^2 + y^2$. The area element $dA = 4dxdy/(1 + K_Gr^2)^2$. For the director field $\mathbf{n} = n_1(x,y)\mathbf{e}_1 + n_2(x,y)\mathbf{e}_2$, where $\mathbf{e}_1$ and $\mathbf{e}_2$ are the orthogonal unit basis vectors, its divergence and curl are div $\mathbf{n} = (1/2)(1 + K_Gr^2)(\partial n_1/\partial x + \partial n_2/\partial y) - K_G(n_1x + n_2y)$, and curl $\mathbf{n} = (1/2)(1 + K_Gr^2)(\partial n_2/\partial x - \partial n_1/\partial y) - K_G(n_2x - n_1y)$, respectively (see Appendix B for the derivation of curl $\mathbf{n}$). We first consider a defect-free uniform director field $(n_1, n_2) = (\cos\theta_0, \sin\theta_0)$ whose associated Lagrange multiplier is $\lambda = K_1K_G(1 + K_Gr^2)$. $\theta_0 \in [0, \pi/2]$. The associated Frank free energy density is independent of θ_0: $f = K_1K_G^2r^2/2$. We see that the uniform state in Poincaré disk has a nonzero energy density that increases with r in a power law. It is due to the special metric structure of the Poincaré disk. Now we consider a $+1$ defect configuration

in the nematic texture on Poincaré disk. It can be characterized by $\mathbf{n} = [(c_2x - c_1y)\mathbf{e}_1 + (c_1x + c_2y)\mathbf{e}_2]/\sqrt{x^2 + y^2}$, where c_1 and c_2 are both constants satisfying $c_1^2 + c_2^2 = 1$, such that the magnitude of $\mathbf{n}$ is unity. Varying the value of c_1 from zero to unity, we obtain director fields from radial to azimuthal configurations. The associated Frank free energy density is

$$f_{+1,h} = \frac{K_1}{2}\frac{(1 - K_Gr^2)^2}{4r^2}. \quad (26)$$

Since $f'_{+1,h}(r) = (K_1/2)(-1 + K^2r^4)/(2r^3) < 0$, the Frank free energy density decreases with r. On the other hand, due to the homogeneity of the Poincaré disk, the optimal position of a $+1$ defect is always at the boundary of the disk.

Finally, we discuss some effects that are not taken into consideration in our calculations. First, by introducing anisotropy in the elastic constants, the free energy varies with the local rotation of the director field. Despite the reduced energy degeneracy arising from the elasticity anisotropy, both radial and azimuthal configurations based on which our calculations are performed are still solutions to the Euler-Lagrange equation (see Appendix C). Therefore, introducing elasticity anisotropy does not change the major conclusions about the optimal positions of both $+1$ and $+1/2$ defects. Second, in addition to curvature, the thickness of liquid-crystal shells is an important parameter to control the number and orientation of defects [5,23]. It has been experimentally observed that thickness variation can produce a number of novel defect configurations over a spherical liquid-crystal shell [5]. It is of great interest to include the effect of thickness in a generalized Frank free energy model to account for these new experimental observations [23]. This is beyond the scope of this study. Third, spatial variations in nematic order parameter within defect cores contribute to the condensation free energy of topological defects [16,17]. Notably, nematic textures in defect core regions can exhibit featured patterns and energy profiles, such as highly biaxial nematic order in the cores of $+1/2$ defects [57] and local melting of the nematic ordering [53]. A recent study has demonstrated that the condensation energy associated with the defect core plays an important role in the formation of defects triggered by strong enough curvature [58]. In our study, we focus on the optimal locations of preexistent defects. They are determined by the variation of the free energy with the positions of the defects, where the contribution from the defect core structures is canceled without considering the boundary effect of defects.

IV. CONCLUSION

In summary, we investigate the curvature-driven stability mechanism of LC defects based on the isotropic nematic disk model where the appearance of defects is not topologically required, and present analytical results on the distinct energy landscape of LC defects created by curvature. We show that with the accumulation of curvature effect both $+1$ and $+1/2$ defects can be stabilized within spherical disks. Specifically, the equilibrium position of the $+1$ defect will move abruptly from the boundary to the center of the spherical disk, exhibiting the first-order phase-transition-like behavior. We also find the alternating repulsive and attractive regimes in the energy curve

of a pair of $+1/2$ defects, which leads to an equilibrium defect pair separation. The sensitive response of defects to curvature and the curvature-driven stability mechanism demonstrated in this work may have implications in the control of LC textures with the dimension of curvature.

APPENDIX A: INFINITE DEGREE OF DEGENERACY IN THE ONE-ELASTIC-CONSTANT APPROXIMATION

Let us consider a planar nematic disk. $\mathbf{n} = [\cos\theta(x,y), \sin\theta(x,y)]$ in Cartesian coordinates. In the one-elastic-constant approximation, the Frank free energy is $F = \frac{1}{2}K_1 \iint_{x^2+y^2 \leqslant r_p^2} |\boldsymbol{\nabla}\theta(x,y)|^2 dx dy$. It is easily seen that rotating a director by a constant angle does not change the Frank free energy.

For a nematic field on a sphere, by inserting $n = [\cos\Psi(\theta,\varphi), \sin\Psi(\theta,\varphi)]$ in spherical coordinates into Eq. (14), we obtain the expression for the Frank free energy density

$$f = \frac{K_1}{2}\left(\frac{1}{R^2\sin^2\theta} + |\boldsymbol{\nabla}\Psi|^2 + \frac{2\cos\theta}{R^2\sin^2\theta}\Psi_\varphi\right),$$

where $\boldsymbol{\nabla}\Psi = \frac{1}{R}\frac{\partial\Psi}{\partial\theta}\mathbf{e}_\theta + \frac{1}{R\sin\theta}\frac{\partial\Psi}{\partial\varphi}\mathbf{e}_\varphi$, and the notation Ψ_φ is an abbreviation for $\partial\Psi/\partial\varphi$. Obviously, the Frank free energy density is invariant under the transformation $\Psi \to \Psi + c$.

The conclusion that the nematic texture has infinite degree of degeneracy in the one elastic constant approximation can be generalized to any generally curved surface by writing the Frank free energy under the one-constant approximation in the form of

$$F = \frac{1}{2}\int dS g^{ij}(\partial_i\alpha - A_i)(\partial_j\alpha - A_j),$$

where the integration is over an area element dS on the surface $\mathbf{x}(u^1, u^2)$, $\alpha(u^1, u^2)$ is the angle between $\mathbf{n}(u^1, u^2)$ and any local reference frame, and A_i is the spin connection [46]. The free energy is invariant under the rotation $\alpha(u^1, u^2) \to \alpha(u^1, u^2) + c$.

APPENDIX B: CALCULATING CURL n ON SPHERICAL GEOMETRY

In a coordinates-independent expression, curl $\mathbf{n} = (\star dn^\flat)^\sharp$ [55,59,60]. The operators $\star$, $\flat$ and $\sharp$ are to be explained below. $\star$ is an operator called Hodge dual. When applied on an antisymmetric tensor $\alpha = \frac{1}{k!}\alpha_{i_1,\cdots,i_k}e^{i_1} \wedge \cdots \wedge e^{i_k}$, where $e^{i_1}, \cdots, e^{i_n}$ are dual bases,

$$\star\alpha = \frac{\sqrt{|g|}\varepsilon_{i_1,\cdots,i_n}\alpha_{j_1,\cdots,j_k}g^{i_1 j_1}\cdots g^{i_k j_k}}{k!(n-k)!}e^{i_{k+1}} \wedge \cdots \wedge e^{i_n}.$$

$\flat$ and $\sharp$ are the musical isomorphisms. $X^\flat = g_{ij}X^i dx^j$, where $X = X^i\partial_i$. $\omega^\sharp = g^{ij}\omega_i\partial_j$, where $\omega = \omega_i dx^i$.

Consider a vector field $\mathbf{n}$ defined on a two-dimensional sphere. $\mathbf{n} = n_1(\theta,\varphi)\mathbf{e}_\theta + n_2(\theta,\varphi)\mathbf{e}_\varphi$, where $\mathbf{e}_\theta$ and $\mathbf{e}_\varphi$ are the unit tangent vectors in spherical coordinates. Applying the above formulas on such a vector field, we have

$$n^\flat = n_1 r d\theta + n_2 r \sin\theta d\varphi,$$

$$dn^\flat = n_1 dr d\theta + n_2 \sin\theta dr d\varphi$$
$$+ r\left(n_2\cos\theta + \sin\theta\frac{\partial n_2}{\partial\theta} - \frac{\partial n_1}{\partial\varphi}\right)d\theta d\varphi,$$

and

$$\star dn^\flat = n_1 \sin\theta d\varphi - n_2 d\theta$$
$$+ \frac{1}{r\sin\theta}\left(n_2\cos\theta + \sin\theta\frac{\partial n_2}{\partial\theta} - \frac{\partial n_1}{\partial\varphi}\right)dr.$$

We finally obtain Eq. (13). It is of interest to note that the curl of a director field $\mathbf{n}$ on a generally curved surface is curl $\mathbf{n} = -\tau_n\mathbf{n} - c_n\mathbf{t} + \kappa_n\boldsymbol{\nu}$, where $\{\mathbf{n}, \mathbf{t}, \boldsymbol{\nu}\}$ constitute the Darboux basis [52]. τ_n and c_n are the components of the extrinsic curvature tensor $\mathbf{L}$. $\mathbf{L}_{nn} = c_n$, and $\mathbf{L}_{nt} = \mathbf{L}_{tn} = -\tau_n$. In general, the extrinsic curvature influences the Frank free energy of nematics on a curved surface. It is only on a flat or spherical surface $\tau_n = 0$ and c_n is a constant. So the extrinsic curvature effect only contributes a constant term in the Frank free energy [52].

APPENDIX C: EULER-LAGRANGE EQUATIONS IN CARTESIAN AND SPHERICAL COORDINATES

In this appendix, we present the Euler-Lagrange equations in Cartesian and spherical coordinates derived from Eq. (3), and show that both radial and azimuthal configurations are solutions to the Euler-Lagrange equations. We also show that the anisotropic elastic constants will not change the main result of curvature-driven alternating repulsive and attractive interactions between the two $+1/2$ defects due to the fact that the elastic modulus K_1 plays no role in the energy expression.

In two-dimensional Cartesian coordinates, $\mathbf{n} = [n_1(x,y), n_2(x,y)]$. The components of the director field in equilibrium nematic textures satisfy the following Euler-Lagrange equations:

$$K_1\left(\frac{\partial^2 n_1}{\partial x^2} + \frac{\partial^2 n_2}{\partial x\partial y}\right) - K_3\left(\frac{\partial^2 n_2}{\partial x\partial y} - \frac{\partial^2 n_1}{\partial y^2}\right) = -\lambda n_1,$$

and

$$K_1\left(\frac{\partial^2 n_2}{\partial y^2} + \frac{\partial^2 n_1}{\partial x\partial y}\right) + K_3\left(\frac{\partial^2 n_2}{\partial x^2} - \frac{\partial^2 n_1}{\partial x\partial y}\right) = -\lambda n_2.$$

It is found that both radial $(n_1, n_2) = (x/\sqrt{x^2+y^2}, y/\sqrt{x^2+y^2})$ and azimuthal $(n_1, n_2) = (-y/\sqrt{x^2+y^2}, x/\sqrt{x^2+y^2})$ configurations satisfy the above Euler-Lagrange equations with $\lambda = K_1/(x^2+y^2)$ and $\lambda = K_3/(x^2+y^2)$, respectively. The spiral configuration $\mathbf{n} = c_1(x/\sqrt{x^2+y^2}, y/\sqrt{x^2+y^2}) + c_2(-y/\sqrt{x^2+y^2}, x/\sqrt{x^2+y^2})$ ($c_1^2 + c_2^2 = 1$ and neither

c_1 nor c_2 is 0) is the solution to the Euler-Lagrange equations only in the one elastic constant approximation.

In spherical coordinates, $\mathbf{n} = n_1\mathbf{e}_\theta + n_2\mathbf{e}_\varphi$. In equilibrium nematic textures, n_1 and n_2 satisfy the following Euler-Lagrange equations:

$$\frac{K_1}{R^2}\left(-\frac{n_1}{\sin^2\theta} + \frac{\partial n_1}{\partial\theta}\frac{\cos\theta}{\sin\theta} + \frac{\partial^2 n_1}{\partial\theta^2} - \frac{\cos\theta}{\sin^2\theta}\frac{\partial n_2}{\partial\varphi}\right.$$
$$\left. + \frac{1}{\sin\theta}\frac{\partial^2 n_2}{\partial\theta\partial\varphi}\right) + \frac{K_3}{r^2\sin^2\theta}\left(\frac{\partial^2 n_1}{\partial\varphi^2} - \frac{\partial n_2}{\partial\varphi}\cos\theta\right.$$
$$\left. - \sin\theta\frac{\partial^2 n_2}{\partial\theta\partial\varphi}\right) = -\lambda n_1,$$

$$\frac{K_3}{R^2}\left(-\frac{n_2}{\sin^2\theta} + \frac{\cos\theta}{\sin^2\theta}\frac{\partial n_1}{\partial\varphi} - \frac{1}{\sin\theta}\frac{\partial^2 n_1}{\partial\theta\partial\varphi} + \frac{\partial^2 n_2}{\partial\theta^2}\right.$$
$$\left. + \frac{\cos\theta}{\sin\theta}\frac{\partial n_2}{\partial\theta}\right) + \frac{K_1}{R^2\sin\theta}\left(\frac{\cos\theta}{\sin\theta}\frac{\partial n_1}{\partial\varphi} + \frac{\partial^2 n_1}{\partial\theta\partial\varphi}\right.$$
$$\left. + \frac{1}{\sin\theta}\frac{\partial^2 n_2}{\partial\varphi^2}\right) = -\lambda n_2.$$

We remark that the equilibrium equations in spherical coordinates are invariant under uniform local rotation of the director field. Similarly, one can show that both radial and azimuthal configurations are solutions to the Euler-Lagrange equations with $\lambda = K_1/(R^2\sin^2\theta)$ and $\lambda = K_3/(R^2\sin^2\theta)$, respectively. The spiral configuration of $n_1 = c_1, n_2 = c_2$ (c_1 and c_2 are nonzero constants satisfying $c_1^2 + c_2^2 = 1$) satisfies the equilibrium equation only when $K_1 = K_3$. For the two $+1/2$ defects configurations discussed in the main text, we show that introducing elasticity anisotropy does not change the curvature-driven alternating repulsive and attractive interactions between the defects. For the two $+1/2$ defects configuration on a spherical disk where an azimuthal configuration is separated by a uniform configuration, the associated Frank free energy is

$$\frac{F_{+\frac{1}{2},s}}{2K_3} = \iint_{D_1}\frac{1}{x^2+y^2}dA + \iint_{D_2}\frac{1}{R^2-y^2}dA,$$

where D_1 and D_2 are given below Eq. (24). We see that since the entire defect configuration is divergence free, the parameter K_3 does not appear in the expression for the Frank free energy. Therefore, anisotropy in elastic constants does not change the featured interaction between the $+1/2$ defects.

[1] H. K. Bisoyi and S. Kumar, Chem. Soc. Rev. **40**, 306 (2011).
[2] G. P. Alexander, B. G.-g. Chen, E. A. Matsumoto, and R. D. Kamien, Rev. Mod. Phys. **84**, 497 (2012).
[3] S. Umadevi, X. Feng, and T. Hegmann, Adv. Funct. Mater. **23**, 1393 (2013).
[4] M. Urbanski, C. G. Reyes, J. Noh, A. Sharma, Y. Geng, V. S. R. Jampani, and J. P. Lagerwall, J. Phys.: Condens. Matter **29**, 133003 (2017).
[5] T. Lopez-Leon, V. Koning, K. Devaiah, V. Vitelli, and A. Fernandez-Nieves, Nature Phys. **7**, 391 (2011).
[6] E. Pairam, J. Vallamkondu, V. Koning, B. C. van Zuiden, P. W. Ellis, M. A. Bates, V. Vitelli, and A. Fernandez-Nieves, Proc. Natl. Acad. Sci. USA **110**, 9295 (2013).
[7] T. Yamamoto and M. Sano, Soft Matter **13**, 3328 (2017).
[8] A. Fernández-Nieves, V. Vitelli, A. S. Utada, D. R. Link, M. Márquez, D. R. Nelson, and D. A. Weitz, Phys. Rev. Lett. **99**, 157801 (2007).
[9] T. Lopez-Leon and A. Fernandez-Nieves, Phys. Rev. E **79**, 021707 (2009).
[10] H.-L. Liang, R. Zentel, P. Rudquist, and J. Lagerwall, Soft Matter **8**, 5443 (2012).
[11] T. Yoshino, M. Kondo, J.-i. Mamiya, M. Kinoshita, Y. Yu, and T. Ikeda, Adv. Mater. **22**, 1361 (2010).
[12] E.-K. Fleischmann, F. R. Forst, and R. Zentel, Macromol. Chem. Phys. **215**, 1004 (2014).
[13] P. G. de Gennes and J. Prost, *The Physics of Liquid Crystals, 2nd ed.* (Oxford University Press, Oxford, 1993).
[14] T. Lopez-Leon and A. Fernandez-Nieves, Colloid Polym. Sci. **289**, 345 (2011).
[15] A. Sengupta, B. Schulz, E. Ouskova, and C. Bahr, Microfluid. Nanofluid. **13**, 941 (2012).
[16] M. Kleman, *Liquid Crystals, Magnetic Systems, and Various Ordered Media* (Wiley, New York, 1983).
[17] P. M. Chaikin and T. C. Lubensky, *Principles of Condensed Matter Physics* (Cambridge University Press, Cambridge, 2000), Vol. 1.
[18] D. R. Nelson, *Defects and Geometry in Condensed Matter Physics* (Cambridge University Press, Cambridge, 2002).
[19] B. L. Mbanga, K. K. Voorhes, and T. J. Atherton, Phys. Rev. E **89**, 052504 (2014).
[20] A. Darmon, M. Benzaquen, S. Čopar, O. Dauchot, and T. Lopez-Leon, Soft Matter **12**, 9280 (2016).
[21] D. R. Nelson, Nano Lett. **2**, 1125 (2002).
[22] M. A. Gharbi, D. Seč, T. Lopez-Leon, M. Nobili, M. Ravnik, S. Žumer, and C. Blanc, Soft Matter **9**, 6911 (2013).
[23] V. Koning, T. Lopez-Leon, A. Darmon, A. Fernandez-Nieves, and V. Vitelli, Phys. Rev. E **94**, 012703 (2016).
[24] J. R. Frank and M. Kardar, Phys. Rev. E **77**, 041705 (2008).
[25] X. Xing, H. Shin, M. J. Bowick, Z. Yao, L. Jia, and M.-H. Li, Proc. Natl. Acad. Sci. USA **109**, 5202 (2012).
[26] B. G.-g. Chen, P. J. Ackerman, G. P. Alexander, R. D. Kamien, and I. I. Smalyukh, Phys. Rev. Lett. **110**, 237801 (2013).
[27] N. Ramakrishnan, P. S. Kumar, and J. H. Ipsen, Biophys. J. **104**, 1018 (2013).
[28] L.M. Pismen, Phys. Rev. E **90**, 060501 (2014).
[29] C. Mostajeran, Phys. Rev. E **91**, 062405 (2015).
[30] M. Leoni, O. Manyuhina, M. Bowick, and M. C. Marchetti, Soft Matter **13**, 1257 (2017).
[31] T. Sanchez, D. T. Chen, S. J. DeCamp, M. Heymann, and Z. Dogic, Nature (London) **491**, 431 (2012).
[32] S. Zhou, A. Sokolov, O. D. Lavrentovich, and I. S. Aranson, Proc. Natl. Acad. Sci. USA **111**, 1265 (2014).
[33] F. C. Keber, E. Loiseau, T. Sanchez, S. J. DeCamp, L. Giomi, M. J. Bowick, M. C. Marchetti, Z. Dogic, and A. R. Bausch, Science **345**, 1135 (2014).

[34] O. D. Lavrentovich, Curr. Opin. Colloid Interface Sci. **21**, 97 (2016).

[35] C. Peng, T. Turiv, Y. Guo, Q.-H. Wei, and O. D. Lavrentovich, Science **354**, 882 (2016).

[36] S. A. Langer and J. P. Sethna, Phys. Rev. A **34**, 5035 (1986).

[37] J. Rudnick and R. Bruinsma, Phys. Rev. Lett. **74**, 2491 (1995).

[38] D. Pettey and T. C. Lubensky, Phys. Rev. E **59**, 1834 (1999).

[39] P. Bhattacharyya, T.-L. Ho, and N. D. Mermin, Phys. Rev. Lett. **39**, 1290 (1977).

[40] D. L. Stein, R. D. Pisarski, and P. W. Anderson, Phys. Rev. Lett. **40**, 1269 (1978).

[41] V. Vitelli and D. R. Nelson, Phys. Rev. E **74**, 021711 (2006).

[42] H. Shin, M. J. Bowick, and X. Xing, Phys. Rev. Lett. **101**, 037802 (2008).

[43] M. A. Bates, J. Chem. Phys. **128**, 104707 (2008).

[44] M. J. Bowick and L. Giomi, Adv. Phys. **58**, 449 (2009).

[45] D. Seč, T. Lopez-Leon, M. Nobili, C. Blanc, A. Fernandez-Nieves, M. Ravnik, and S. Žumer, Phys. Rev. E **86**, 020705 (2012).

[46] V. Vitelli and D. R. Nelson, Phys. Rev. E **70**, 051105 (2004).

[47] V. Koning and V. Vitelli, *Fluids, Colloids and Soft Materials: An Introduction to Soft Matter Physics* (Wiley, New York, 2016), pp. 369–386.

[48] C. M. Knobler and R. C. Desai, Annu. Rev. Phys. Chem. **43**, 207 (1992).

[49] J. Fang, E. Teer, C. M. Knobler, K.-K. Loh, and J. Rudnick, Phys. Rev. E **56**, 1859 (1997).

[50] R. K. Gupta and V. Manjuladevi, Isr. J. Chem. **52**, 809 (2012).

[51] J. Xue, C.S. Jung, and M. W. Kim, Phys. Rev. Lett. **69**, 474 (1992).

[52] G. Napoli and L. Vergori, Phys. Rev. Lett. **108**, 207803 (2012).

[53] S. Kralj, R. Rosso, and E. G. Virga, Soft Matter **7**, 670 (2011).

[54] R. Rosso, E. G. Virga, and S. Kralj, Continuum Mech. Thermodyn. **24**, 643 (2012).

[55] M. Nakahara, *Geometry, Topology and Physics* (CRC Press, Boca Raton, 2003).

[56] C. D. Modes and R. D. Kamien, Phys. Rev. Lett. **99**, 235701 (2007).

[57] N. Schopohl and T. J. Sluckin, Phys. Rev. Lett. **59**, 2582 (1987).

[58] L. Mesarec, W. Góźdź, A. Iglič, and S. Kralj, Sci. Rep. **6**, 27117 (2016).

[59] M. Berger, *A Panoramic View of Riemannian Geometry* (Springer Science & Business Media, Berlin, 2012).

[60] P. Mikusinski and M. Taylor, *An Introduction to Multivariable Analysis from Vector to Manifold* (Springer Science & Business Media, Berlin, 2012).